Letter

Large Area, Few-Layer Graphene Films on Arbitrary Substrates by Chemical Vapor Deposition

Alfonso Reina, Xiaoting Jia, John Ho, Daniel Nezich, Hyungbin Son, Vladimir Bulovic, Mildred S. Dresselhaus, and Jing Kong

More About This Article

Additional resources and features associated with this article are available within the HTML version:

- Supporting Information
- Access to high resolution figures
- Links to articles and content related to this article
- Copyright permission to reproduce figures and/or text from this article

View the Full Text HTML

ACS Publications
High quality. High impact.

Large Area, Few-Layer Graphene Films on Arbitrary Substrates by Chemical Vapor Deposition

Alfonso Reina,[†] Xiaoting Jia,[†] John Ho,[‡] Daniel Nezich,[§] Hyungbin Son,[‡] Vladimir Bulovic,[‡] Mildred S. Dresselhaus,[‡,§] and Jing Kong*,[‡]

Department of Materials Science and Engineering, Department of Electrical Engineering and Computer Science, Department of Physics, Massachusetts Institute of Technology, Cambridge, Massachusetts 02139

ABSTRACT

In this work we present a low cost and scalable technique, via ambient pressure chemical vapor deposition (CVD) on polycrystalline Ni films, to fabricate large area (~cm²) films of single- to few-layer graphene and to transfer the films to nonspecific substrates. These films consist of regions of 1 to ~12 graphene layers. Single- or bilayer regions can be up to 20 μm in lateral size. The films are continuous over the entire area and can be patterned lithographically or by prepatterning the underlying Ni film. The transparency, conductivity, and ambipolar transfer characteristics of the films suggest their potential as another materials candidate for electronics and opto-electronic applications.

Graphene is the hexagonal arrangement of carbon atoms forming a one-atom thick planar sheet. The successful isolation of graphene by the microcleaving of highly oriented pyrolytic graphite (HOPG)[1] has opened up exciting possibilities for experimental investigations.[2,3] Significant attention has been captured by its outstanding properties which render it another materials option for electronics applications.[4−9] Chemical routes to fabricate graphene may offer significant advantages over the microcleaving of HOPG[10−14] when pursuing the coverage of large substrate areas with graphene for large scale applications. Methods for large area graphene synthesis include ultrahigh vacuum (UHV) annealing of single-crystal SiC (0001),[13,15] UHV chemical vapor deposition (CVD) on single crystal transition metals[12] and the deposition of graphene oxide (GO) films from a liquid suspension followed by chemical reduction.[10,16] However, some of these approaches require the use of a specific substrate material. Furthermore, the high cost of the single crystal substrates and the UHV conditions necessary for growth significantly limit the use of these methods for large scale applications. Films derived from liquid suspensions of graphene flakes can potentially overcome these limitations but the intrinsic properties of graphene have not yet been achieved.[10,17−19] In the present work, we use ambient-pressure CVD to synthesize single- to few layer graphene films on evaporated polycrystalline Ni. Because of the use of ambient pressure and readily available Ni films, this process enables the inexpensive and high-throughput growth of graphene over large areas with properties closer to those found by microcleaving HOPG. Additionally, our method allows the flexibility of transferring the produced film to alternative substrates by wet-etching the Ni film. The graphene films can then be used without further treatment and exhibit outstanding properties in terms of optical transparency and electrical conductivity. The graphene film can be patterned by standard lithographic processes. Alternatively, the catalytic Ni surface can be prepatterned in order to produce graphene patterns of desired geometries at controlled locations.

The growth of graphene monolayers on single crystalline transition metals such as Co,[20] Pt,[21,22] Ir,[23,24] Ru,[25,26] and Ni[27−31] is well known. The nucleation and growth of graphene usually occurs by exposure of the transition metal surface to a hydrocarbon gas under low pressure or UHV conditions. In our CVD process, we expose a polycrystalline Ni film (at 900−1000 °C) to a highly diluted hydrocarbon flow under ambient pressure (see Supporting Information). This gives rise to an ultrathin graphene film (1 to ~10 layers) over the Ni surface. The Ni films were e-beam evaporated onto SiO₂/Si substrates and thermally annealed before the CVD synthesis (see Supporting Information). Thermal annealing before the CVD process generates a Ni film microstructure with single-crystalline grains of sizes between 1 μm to 20 μm. The surfaces of these grains have atomically flat terraces and steps, similar to the surface of single crystal

---

* To whom correspondence should be addressed. E-mail: jingkong@mit.edu.
  † Department of Materials Science and Engineering.
  ‡ Department of Electrical Engineering and Computer Science.
  § Department of Physics.
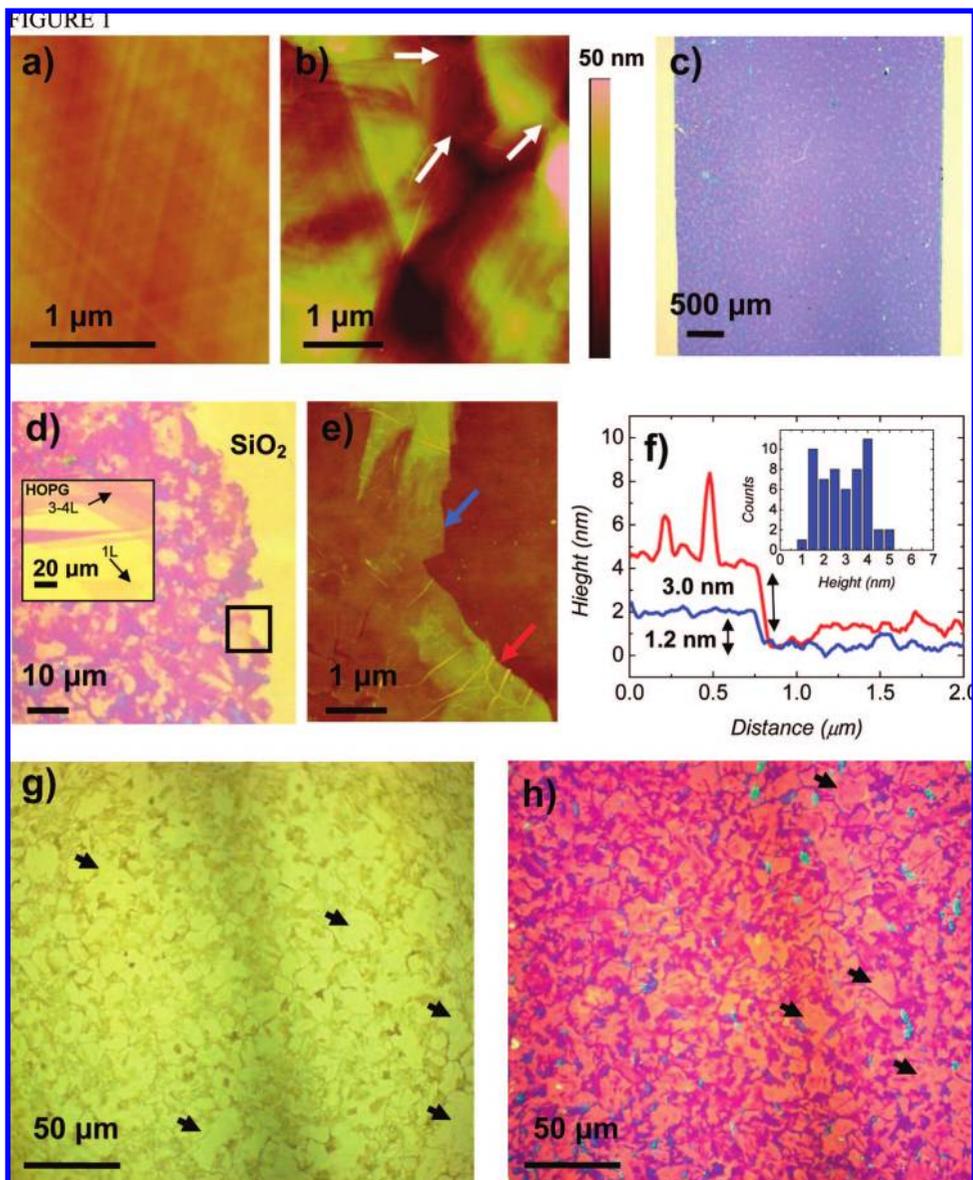
Figure 1. Graphene films grown by CVD on Ni. (a) AFM image of the surface of a Ni grain with atomically flat terraces and steps after annealing. (b) AFM image of a graphene film on polycrystalline Ni after CVD synthesis. The ripples (pointed out by white arrows) at the edge of the groove indicate that the film growth bridges across the gaps between grains. (c) Optical image of a CVD-grown graphene film (blue) transferred to a SiO₂/Si substrate (yellow background). The size of the graphene film is determined by the size of the initial Ni substrate. (d) Optical image of an edge of a graphene film on a SiO₂/Si substrate. Graphene on SiO₂/Si obtained by HOPG cleaving is shown in the inset for comparison. (e) AFM image of the region enclosed by the black square in panel d. The blue (red) arrow corresponds to the pink (purple) region in panel d. (f) Height measurements on the two positions indicated in panel e. The blue (red) curve corresponds to the region identified by the blue (red) arrow in panel e. The height distribution, measured by AFM images taken from the film edge in panel d, is shown as an inset. (g) Optical image of a Ni film after the CVD process and with a graphene film on its surface. (h) Optical image of the same graphene film in panel g transferred to a SiO₂/Si substrate showing a high density of large regions (1−20 μm) consisting of 1−2 layers of graphene (identified by the black arrows). These regions grow on the large Ni grains, identified by the arrows in panel g. The morphology (shape and size) of graphene regions with constant thickness resemble the morphology of the Ni grains in panel g. Color scale bar corresponds to panels a,b.

substrates used for epitaxial UHV graphene growth[12,13] (Figure 1a). In this way, the growth of graphene on the surface of individual Ni grains resembles the growth of graphene on the surface of a single crystal substrate. In our CVD process, graphene growth is likely to occur due to the precipitation of graphite from carbon species within the Ni film as observed for other transition metals, such as Ru.[12] During the exposure of the Ni surface to a H₂ and CH₄ gas mixture in atmospheric conditions, the Ni film and the carbon atoms provided by this CVD process form a solid solution. Since the solubility of carbon in Ni is temperature-dependent, carbon atoms precipitate as a graphene layer on the Ni surface upon cooling of the sample. Because of the formation of grain boundaries, the top surface of the Ni film becomes discontinuous after the thermal annealing. Nevertheless, we found that single- and few- layer graphene bridges across these gaps, thus forming a continuous film over the entire Ni area (see arrows in Figure 1b).
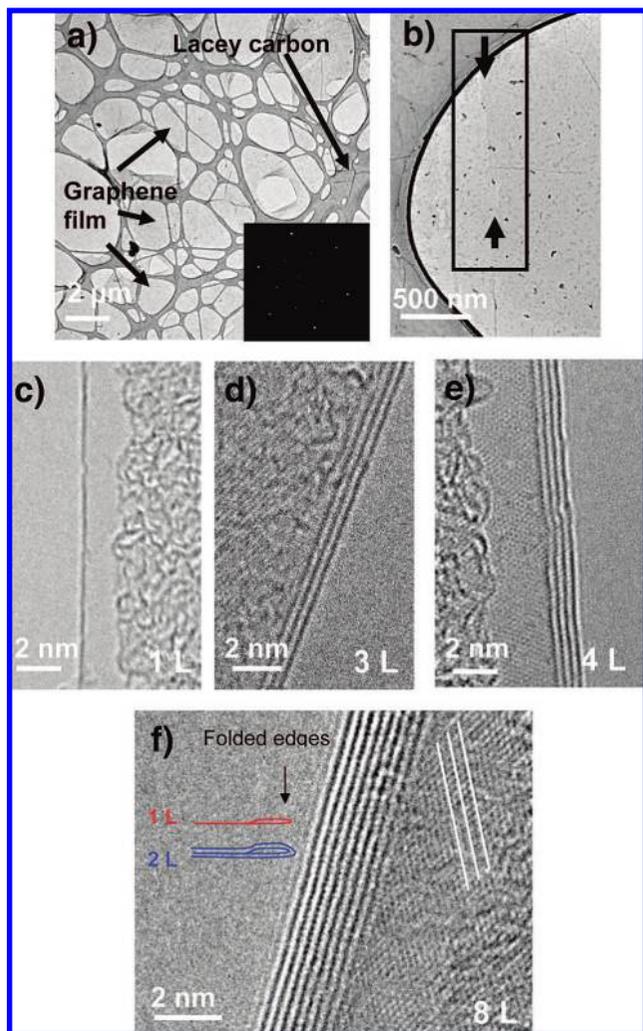
Figure 2. TEM characterization of CVD-grown graphene films. (a) Low-magnification TEM image showing a CVD-grown graphene film on a lacey carbon-coated grid. Electron diffraction on the graphene film is shown as an inset. (b) Low-magnification TEM image showing the interface between areas with different thickness (identified by the black arrow). Although the color contrast is high under optical images, the low contrast in TEM images shows that the thickness difference is only a few graphene layers. (c−f) High-magnification TEM images showing the edges of film regions consisting of one (c), three (d), four (e), and eight (f) graphene layers. The cross-sectional view is enabled by the folding of the film edge. The in-plane lattice fringes suggest local stacking order of the graphene layers.

The transfer of the CVD-derived graphene films to a nonspecific substrate is enabled by the wet-etching of the underlying Ni film. This is carried out by treating the film with an aqueous HCl solution after a support material is coated on the Ni/graphene surface, in our case a poly[methyl methacrylate] (PMMA) layer (see Supporting Information). This results in a free-standing PMMA/graphene membrane that can be handled easily and placed on the desired target substrate (graphene facing the surface).[32] Finally, the PMMA can be dissolved with acetone to yield a graphene film on the desired substrate. The transferred graphene films preserve their continuity and attach strongly to substrates made of almost any material, such as semiconductors, glass, metals and plastics, via van der Waals interactions. In the case of SiO$_2$/Si substrates, the
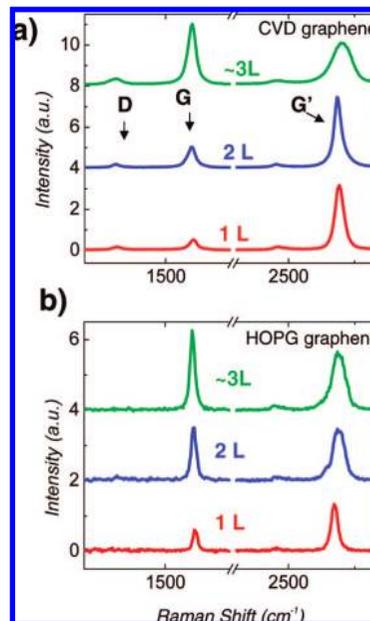
Figure 3. Raman spectroscopy of CVD-grown graphene films on SiO$_2$/Si. (a) Raman spectra of 1 (red), 2 (blue), and ~3 (green) graphene layers from a CVD graphene film. (b) Raman spectra of 1 (red), 2 (blue), and 3 (green) graphene layers derived by the microcleaving of HOPG for comparison. The excitation wavelength is 532 nm.

attached graphene films can successfully withstand harsh processing procedures, such as sonication or acidic treatment. The size and shape of the transferred graphene film on the new substrate are defined by the dimensions of the initial Ni-coated substrate (Figure 1c).

Important morphological film features are revealed by optical images when the films are on Si substrates with a 300 nm oxide layer (Figure 1d). Variations in the film thickness are indicated by the change of color contrast in the optical images, due to light interference on the SiO$_2$ layer modulated by the graphene layers.[33,34] The differences in thickness range from a monolayer to a few graphene layers. The lightest pink regions in the optical images (Figure 1d) have a thickness of roughly 1 nm, as measured by AFM (Figure 1e,f), which typically corresponds to a monolayer or bilayer of graphene.[35,36] Purple regions correspond to 3 nm thickness. Height measurements extracted from a series of AFM images along the film edge in Figure 1d show that the thickness ranges from 1 to 5 nm (inset of Figure 1f with an average of 2.8 nm ± 0.3), corresponding to approximately 1−12 graphene layers.[35] Furthermore, the mean and the rms roughness estimated with our AFM data are 1.97 and 3.27 nm, respectively, over a 100 μm^2 area (see Supporting Information). By comparing optical images of as-grown graphene films on the Ni surface and their images after being transferred to SiO$_2$/Si (Figure 1g,h), we observe that the morphologies of the graphene film correlate qualitatively with the microstructure of the Ni films. For example, we observe a high density of regions with only 1−2 graphene layers in thickness and 1−20 μm in lateral dimensions (black arrows in Figure 1h). Further analysis (see Supporting Information) confirms that these regions usually grow on the surface of
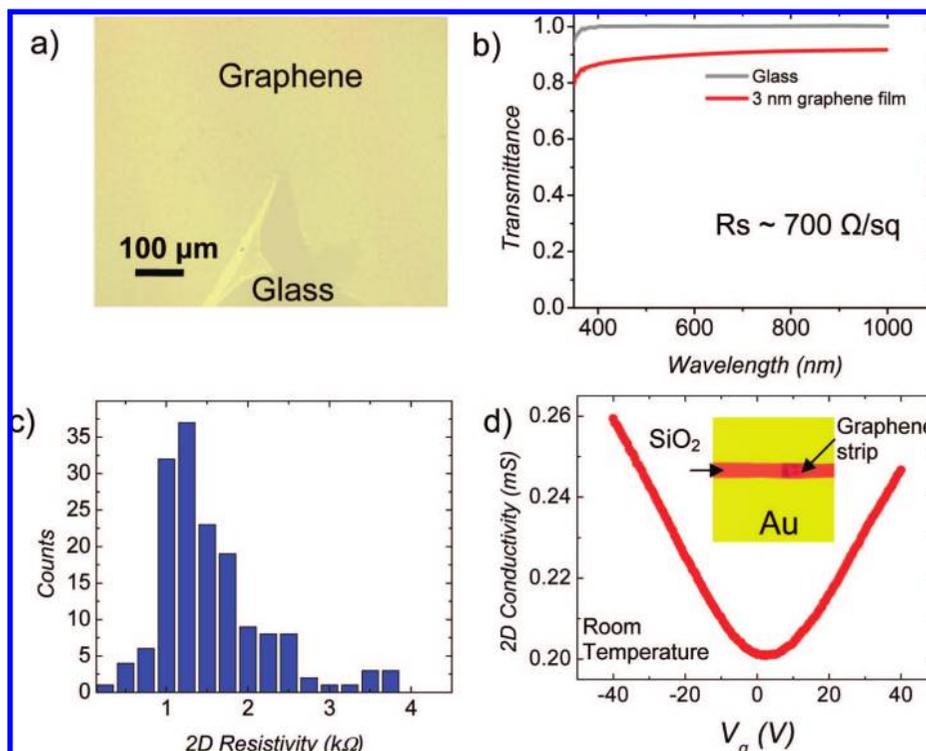
Figure 4. Optical and electrical characterization of CVD graphene films and devices. (a) Optical image of a graphene film transferred to a glass substrate. The broken edge on the bottom can be used to recognize the film. (b) Optical transmittance of a graphene film with 3 nm average thickness on glass. (c) Histogram of the 2D resistivity (kΩ) (resistance of each device normalized by its length and width) of ~100 graphene film devices prepared by the CVD process. (d) 2D conductivity vs gate voltage of a graphene film transistor. An optical image of a graphene strip device is shown as an inset.

large Ni grains that have similar lateral sizes (black arrows in Figure 1g). These observations imply that individual nickel grains may independently affect the thickness of the graphene film during CVD, leading to the thickness variations we observe on our films. Similarly, our observations suggest that most of the multilayer graphene nucleation occurs at the grain boundaries. This could be explained by the fact that at such boundaries, there is a higher density of atomic steps due to the curvature of the grain edge, thereby inducing the nucleation of several graphene layers.[12] This points to future work on controlling the morphology of the Ni films in order to optimize the morphology of the graphene films.

The CVD grown films can be transferred by the same method to TEM lacey carbon-coated grids (Figure 2a,b). TEM examination confirms that changes in film thickness correspond to only a few graphene layers. The edges of the suspended film always fold back, allowing for a cross-sectional view of the film. The observation of these edges by TEM provides an accurate way to measure the number of layers at multiple locations on the film (Figure 2c−f). Typically, sections of 1−8 layers are observed in our samples in close agreement with our AFM data. The estimated interlayer spacing is 3.50 ± 0.14 Å. Electron diffraction on the graphene film (inset of Figure 2a) reveals a hexagonal pattern confirming the three-fold symmetry of the arrangement of carbon atoms (the beam size used was 50 nm). When different regions of the film are inspected, well-defined diffraction spots (instead of ring patterns) are always observed (see Supporting Information), indicating the crystallinity of all regions examined. Stacking disorder of

graphene layers in multilayer regions is suggested by the appearance of electron diffraction spots misaligned with respect to each other (see Supporting Information). The observation of lattice fringes (Figure 2d−f) on the in-plane direction of the graphene sheets is possible. The in-plane lattice constant is measured to be 2.32 ± 0.48 Å (compared to 2.46 Å for graphite[37]).

Raman spectroscopy provides a quick and facile structural and quality characterization of the produced material. Figure 3 compares the Raman spectra of 1, 2, and 3 graphene layers derived by CVD and by HOPG. A low intensity of the disorder-induced D band (~1350 cm^{-1}) is observed by plotting I_D/I_G, the D to G (~1580 cm^{-1}) peak intensity ratios, where G denotes the symmetry-allowed graphite band, obtaining $0.05 < I_D/I_G < 0.3$. Some weak D band intensity is observed also away from graphene edges, suggesting the existence of subdomain boundaries in areas with a constant number of graphene layers. Spectra from the thinnest sections of the CVD graphene film show a sharp line width (~30 cm^{-1}) and a single Lorentzian profile of the G′ band (~2700 cm^{-1}), which are hallmarks of monolayer graphene.[38] The G′ line shape provides a good measure of the number of layers in the case of HOPG-derived graphene.[38] However, we observe that in multilayer (>1 graphene layers) CVD graphene there is a variation in the G′ line shape between regions of identical layer number. Moreover, sections of ~2 L and 3 L regions can show linewidths of ~30 cm^{-1} and single-Lorentzian lineshapes. This indicates that an ordered stacking (i.e., ABAB stacking) and therefore an electronic coupling between graphene layers may not occur in all regions
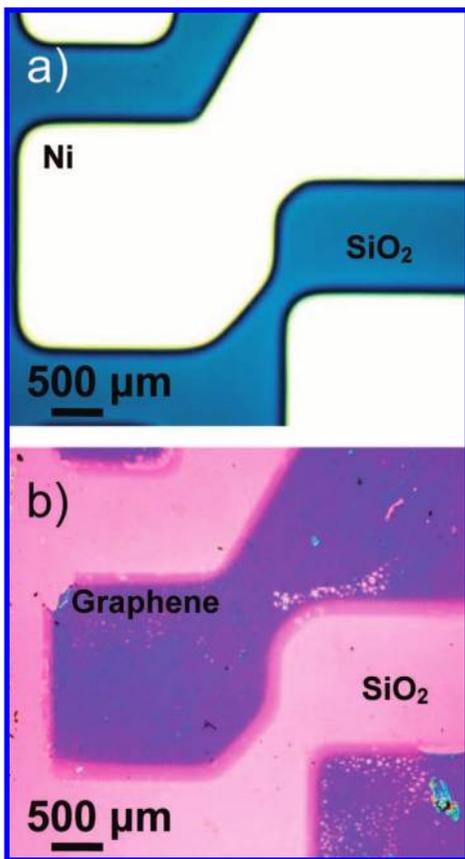
Figure 5. Direct growth of graphene patterns from prepatterned Ni structures. (a) Optical image of a prepatterned Ni film on SiO_2/Si. CVD graphene is grown on the surface of the Ni pattern. (b) Optical image of the grown graphene transferred from the Ni surface in panel a to another SiO_2/Si substrate.

of the film, or to the same degree as in HOPG. This observation is consistent with our electron diffraction spectra. The absence of interlayer coupling may be a positive effect since incommensurate, multilayer graphene can have electronic properties similar to those of a single sheet of graphene.[39] Instead of the G′ line shape, we have found that the G to G′ peak intensity ratios ($I_G/I_{G'}$) provide a good correlation with the number of graphene layers in the CVD graphene samples (see Supporting Information).

The intrinsic quality of the CVD graphene films makes them excellent candidates for both optoelectronic and electronic applications. Figure 4a is an optical image of the graphene film transferred onto a glass substrate. With a film having 3 nm average thickness, the optical transmittance is ∼90% in the 500−1000 nm wavelength regime (Figure 4b). The sheet resistances (R_s) of the films are 770 −1000 Ω/sq as measured by a four-point probe instrument.

We further characterized the electrical properties by fabricating graphene transistors. Photolithography and O_2 plasma etching were used to pattern graphene films in 2−8 μm stripes. Transistor channel lengths ranged from 5−15 μm. Figure 4c is a histogram of the 2D resistivity obtained by measuring ∼100 devices at 0 V gate voltage. By applying a gate voltage of up to ± 40 V (provided by a Si back gate with 300 nm oxide thickness), the conductance values of the stripes are modulated by 1.3∼2 times (Figure 4d). This indicates that the

effect of gate modulation is not as effective as it is in other graphene transistors made by microcleaving HOPG.[40] The inset in Figure 4d shows an optical image of a typical device. The average thickness of the graphene strip of this device is also estimated to be ∼3 nm. Because of thickness variation, it is possible that the gating effect is screened by other graphene layers in multilayer regions of the film.[2,41] Mobility values can be derived from the slope of the conductivity variation with gate voltage. These range from 100 to 2000 cm^2/ V sec for both electrons and holes, which are ∼2 orders of magnitude lower than the best reported graphene mobilities on substrates. This is possibly due to an ineffective gate coupling or to grain boundary scattering inside the graphene strip. Efforts are underway to improve the quality of the films by tuning the CVD growth conditions.

The ability to grow single and few-layer graphene with CVD is an important advantage. Analogous to the case of carbon nanotube growth,[42,43] this technique can potentially enable the simple growth of graphene at particular locations and with desired geometries by controlling the catalyst morphology and position.[44] Figure 5 demonstrates the direct CVD growth of a graphene pattern using a prepatterned Ni structure (Figure 5a). After CVD, the graphene is transferred to a SiO_2/Si substrate (Figure 5b) with a process similar to the one described previously (see Supporting Information). This is a significant addition to the capabilities of graphene device fabrication and integration. For example, in the case of O_2 plasma-sensitive substrates or substrates which cannot withstand the lithographic processes, graphene devices can be patterned through this approach.

In summary, we have demonstrated for the first time that continuous films with single- to few-layer graphene can be grown by ambient pressure CVD on polycrystalline Ni and transferred to a large variety of substrates. The films exhibit a large fraction of single- and bilayer graphene regions with up to ∼20 μm in lateral size. They remain continuous and conductive after numerous processing steps, even though the thinnest parts are only one monolayer in thickness. These films demonstrate a comparable structural quality to existing graphene materials but are fabricated without the need of bulk single crystal substrates or complex processing conditions. The graphene film size is determined by the area of the Ni growth surface and is only limited by the CVD chamber size. Furthermore, our studies suggest that the polycrystalline structure of the Ni film plays an important role in the formation of the graphene film morphology. With better engineering of the Ni film, such as enlarging and controlling the location of the single crystal grains, well-controlled graphene features can be envisioned. This approach enables a viable route toward the scalable production of graphene structures for future applications.

Note Added after ASAP Publication: This paper was published ASAP on December 1, 2008. Two Supporting Information files were removed from the Web and the paper was reposted on December 29, 2008.

Supporting Information Available: A detailed description of the fabrication methods. This material is available free of charge via the Internet at http://pubs.acs.org.

References

(1) Novoselov, K. S.; Jiang, D.; Schedin, F.; Booth, T. J.; Khotkevich, V. V.; Morozov, S. V.; Geim, A. K. Two-dimensional atomic crystals. *Proc. Natl. Acad. Sci. U.S.A.* **2005**, *102* (30), 10451–10453.

(2) Novoselov, K. S.; Geim, A. K.; Morozov, S. V.; Jiang, D.; Katsnelson, M. I.; Grigorieva, I. V.; Dubonos, S. V.; Firsov, A. A. Two-dimensional gas of massless Dirac fermions in graphene. *Nature* **2005**, *438* (7065), 197–200.

(3) Zhang, Y. B.; Tan, Y. W.; Stormer, H. L.; Kim, P. Experimental observation of the quantum Hall effect and Berry's phase in graphene. *Nature* **2005**, *438* (7065), 201–204.

(4) Schedin, F.; Geim, A. K.; Morozov, S. V.; Hill, E. W.; Blake, P.; Katsnelson, M. I.; Novoselov, K. S. Detection of individual gas molecules adsorbed on graphene. *Nat. Mater.* **2007**, *6* (9), 652–655.

(5) Oostinga, J. B.; Heersche, H. B.; Liu, X.; Morpurgo, A. F.; Vandersypen, L. M. K. Gate-induced insulating state in bilayer graphene devices. *Nat. Mater.* **2008**, *7* (2), 151–157.

(6) Ohta, T.; Bostwick, A.; Seyller, T.; Horn, K.; Rotenberg, E. Controlling the electronic structure of bilayer graphene. *Science* **2006**, *313* (5789), 951–954.

(7) Miao, F.; Wijeratne, S.; Zhang, Y.; Coskun, U. C.; Bao, W.; Lau, C. N. Phase-Coherent Transport in Graphene Quantum Billiards. *Science* **2007**, *317* (5844), 1530–1533.

(8) Wang, F.; Zhang, Y.; Tian, C.; Girit, C.; Zettl, A.; Crommie, M.; Shen, Y. R. Gate-Variable Optical Transitions in Graphene. *Science* **2008**, *320* (5873), 206–209.

(9) Bolotin, K. I.; Sikes, K. J.; Jiang, Z.; Klima, M.; Fudenberg, G.; Hone, J.; Kim, P.; Stormer, H. L. Ultrahigh electron mobility in suspended graphene. *Solid State Commun.* **2008**, *146* (9−10), 351–355.

(10) Eda, G.; Fanchini, G.; Chhowalla, M. Large-area ultrathin films of reduced graphene oxide as a transparent and flexible electronic material. *Nat. Nanotechnol.* **2008**, *3* (5), 270–274.

(11) Li, D.; Muller, M. B.; Gilje, S.; Kaner, R. B.; Wallace, G. G. Processable aqueous dispersions of graphene nanosheets. *Nat. Nanotechnol.* **2008**, *3* (2), 101–105.

(12) Sutter, P. W.; Flege, J.-I.; Sutter, E. A. Epitaxial graphene on ruthenium. *Nat. Mater.* **2008**, *7* (5), 406–411.

(13) Berger, C.; Song, Z. M.; Li, X. B.; Wu, X. S.; Brown, N.; Naud, C.; Mayo, D.; Li, T. B.; Hass, J.; Marchenkov, A. N.; Conrad, E. H.; First, P. N.; de Heer, W. A. Electronic confinement and coherence in patterned epitaxial graphene. *Science* **2006**, *312* (5777), 1191–1196.

(14) Liang, X.; Fu, Z.; Chou, S. Y. Graphene Transistors Fabricated via Transfer-Printing In Device Active-Areas on Large Wafer. *Nano Lett.* **2007**, *7* (12), 3840–3844.

(15) Berger, C.; Song, Z. M.; Li, T. B.; Li, X. B.; Ogbazghi, A. Y.; Feng, R.; Dai, Z. T.; Marchenkov, A. N.; Conrad, E. H.; First, P. N.; de Heer, W. A. Ultrathin epitaxial graphite: 2D electron gas properties and a route toward graphene-based nanoelectronics. *J. Phys. Chem. B* **2004**, *108* (52), 19912–19916.

(16) Stankovich, S.; Dikin, D. A.; Piner, R. D.; Kohlhaas, K. A.; Kleinhammes, A.; Jia, Y.; Wu, Y.; Nguyen, S. T.; Ruoff, R. S. Synthesis of graphene-based nanosheets via chemical reduction of exfoliated graphite oxide. *Carbon* **2007**, *45* (7), 1558–1565.

(17) Wang, X.; Zhi, L. J.; Mullen, K. Transparent, conductive graphene electrodes for dye-sensitized solar cells. *Nano Lett.* **2008**, *8* (1), 323–327.

(18) Li, X.; Zhang, G.; Bai, X.; Sun, X.; Wang, X.; Wang, E.; Dai, H. Highly conducting graphene sheets and Langmuir-Blodgett films. *Nat. Nanotechnol.* **2008**, *3* (9), 538–542.

(19) Hernandez, Y.; Nicolosi, V.; Lotya, M.; Blighe, F. M.; Sun, Z.; De, S.; McGovern, I. T.; Holland, B.; Byrne, M.; Gun'Ko, Y. K.; Boland, J. J.; Niraj, P.; Duesberg, G.; Krishnamurthy, S.; Goodhue, R.; Hutchison, J.; Scardaci, V.; Ferrari, A. C.; Coleman, J. N. High-yield production of graphene by liquid-phase exfoliation of graphite. *Nat. Nanotechnol.* **2008**, *3* (9), 563–568.

(20) Vaari, J.; Lahtinen, J.; Hautojärvi, P. The adsorption and decomposition of acetylene on clean and K-covered Co(0001). *Catal. Lett.* **1997**, *44* (1), 43–49.

(21) Ueta, H.; Saida, M.; Nakai, C.; Yamada, Y.; Sasaki, M.; Yamamoto, S. Highly oriented monolayer graphite formation on Pt(111) by a supersonic methane beam. *Surf. Sci.* **2004**, *560* (1−3), 183–190.

(22) Starr, D. E.; Pazhetnov, E. M.; Stadnichenko, A. I.; Boronin, A. I.; Shaikhutdinov, S. K. Carbon films grown on Pt(111) as supports for model gold catalysts. *Surf. Sci.* **2006**, *600* (13), 2688–2695.

(23) Gall′, N.; Rut'kov, E.; Tontegode, A. Interaction of silver atoms with iridium and with a two-dimensional graphite film on iridium: Adsorption, desorption, and dissolution. *Phys. Solid State* **2004**, *46* (2), 371–377.

(24) Coraux, J.; Ndiaye, A. T.; Busse, C.; Michely, T. Structural Coherency of Graphene on Ir(111). *Nano Lett.* **2008**, *8* (2), 565–570.

(25) de Parga, A. L. V.; Calleja, F.; Borca, B.; Passeggi, J. M. C. G.; Hinarejos, J. J.; Guinea, F.; Miranda, R. Periodically Rippled Graphene: Growth and Spatially Resolved Electronic Structure. *Phys. Rev. Lett.* **2008**, *100* (5), 056807–4.

(26) Marchini, S.; Gunther, S.; Wintterlin, J. Scanning tunneling microscopy of graphene on Ru(0001). *Phys. Rev. B Condens. Matter* **2007**, *76* (7), 075429–9.

(27) Goodman, D. W.; Yates, J. T. CO isotopic mixing measurements on nickel: Evidence for irreversibility of CO dissociation. *J. Catal.* **1983**, *82* (2), 255–260.

(28) Madden, H. H.; Kuppers, J.; Ertl, G. Interaction of carbon monoxide with (110) nickel surfaces. *J. Chem. Phys.* **1973**, *58* (8), 3401–3410.

(29) Gamo, Y.; Nagashima, A.; Wakabayashi, M.; Terai, M.; Oshima, C. Atomic structure of monolayer graphite formed on Ni(111). *Surf. Sci.* **1997**, *374* (1−3), 61–64.

(30) Kawano, T.; Kawaguchi, M.; Okamoto, Y.; Enomoto, H.; Bando, H. Preparation of layered B/C/N thin films on nickel single crystal by LPCVD. *Solid State Sci.* **2002**, *4* (11−12), 1521–1527.

(31) Starodubov, A. G.; Medvetskii, M. A.; Shikin, A. M.; Adamchuk, V. K. Intercalation of silver atoms under a graphite monolayer on Ni(111). *Phys. Solid State* **2004**, *46* (7), 1340–1348.

(32) Reina, A.; Son, H.; Jiao, L.; Fan, B.; Dresselhaus, M. S.; Liu, Z.; Kong, J. Transferring and Identification of Single- and Few-Layer Graphene on Arbitrary Substrates. *J. Phys. Chem. C* **2008**.

(33) Abergel, D. S. L.; Russell, A.; Fal'ko, V. I. Visibility of graphene flakes on a dielectric substrate. *Appl. Phys. Lett.* **2007**, *91* (6), 063125–3.

(34) Blake, P.; Hill, E. W.; Neto, A. H. C.; Novoselov, K. S.; Jiang, D.; Yang, R.; Booth, T. J.; Geim, A. K. Making graphene visible. *Appl. Phys. Lett.* **2007**, *91* (6), 063124–3.

(35) Gupta, A.; Chen, G.; Joshi, P.; Tadigadapa, S.; Eklund, P. C. Raman scattering from high-frequency phonons in supported *n*-graphene layer films. *Nano Lett.* **2006**, *6* (12), 2667–2673.

(36) Li, X.; Wang, X.; Zhang, L.; Lee, S.; Dai, H. Chemically Derived, Ultrasmooth Graphene Nanoribbon Semiconductors. *Science* **2008**, *319* (5867), 1229–1232.

(37) Baskin, Y.; Meyer, L. Lattice Constants of Graphite at Low Temperatures. *Phys. Rev.* **1955**, *100* (2), 544.

(38) Ferrari, A. C.; Meyer, J. C.; Scardaci, V.; Casiraghi, C.; Lazzeri, M.; Mauri, F.; Piscanec, S.; Jiang, D.; Novoselov, K. S.; Roth, S.; Geim, A. K. Raman Spectrum of Graphene and Graphene Layers. *Phys. Rev. Lett.* **2006**, *97* (18), 187401–4.

(39) Hass, J.; Varchon, F.; Millan-Otoya, J. E.; Sprinkle, M.; Sharma, N.; de Heer, W. A.; Berger, C.; First, P. N.; Magaud, L.; Conrad, E. H. Why Multilayer Graphene on 4H-SiC(0001̄) Behaves Like a Single Sheet of Graphene. *Phys. Rev. Lett.* **2008**, *100* (12), 125504–4.

(40) Chen, J.-H.; Jang, C.; Xiao, S.; Ishigami, M.; Fuhrer, M. S. Intrinsic and extrinsic performance limits of graphene devices on SiO₂. *Nat. Nanotechnol.* **2008**, *3* (4), 206–209.

(41) Novoselov, K. S.; Geim, A. K.; Morozov, S. V.; Jiang, D.; Zhang, Y.; Dubonos, S. V.; Grigorieva, I. V.; Firsov, A. A. Electric Field Effect in Atomically Thin Carbon Films. *Science* **2004**, *306* (5696), 666–669.

(42) Kong, J.; Soh, H. T.; Cassell, A. M.; Quate, C. F.; Dai, H. Synthesis of individual single-walled carbon nanotubes on patterned silicon wafers. *Nature* **1998**, *395* (6705), 878–881.

(43) Hayamizu, Y.; Yamada, T.; Mizuno, K.; Davis, R. C.; Futaba, D. N.; Yumura, M.; Hata, K. Integrated three-dimensional microelectromechanical devices from processable carbon nanotube wafers. *Nat. Nanotechnol.* **2008**, *3* (5), 289–294.

(44) Sutter, E. P. S. Au-Induced Encapsulation of Ge Nanowires in Protective C Shells. *Adv. Mater.* **2006**, *18* (19), 2583–2588.

NL801827V